

Effect of concurrent use of whole-body vibration and parathyroid hormone on bone structure and material properties of ovariectomized mice

Takeshi Matsumoto^{1,2}, Shinya Itamochi², Yoshihiro Hashimoto²

¹*Department of Mechanical Engineering, Tokushima University Graduate School of Advanced
Technology and Science, Tokushima, Japan*

²*Department of Mechanical Science and Bioengineering, Osaka University Graduate School of
Engineering Science, Toyonaka Japan*

Corresponding author: Takeshi Matsumoto, PhD

Tel/Fax: +81 88 656 7374

Email: t.matsumoto@tokushima-u.ac.jp

Department of Mechanical Engineering, Tokushima University Graduate School of Advanced
Technology and Science, 2-1 Minamijosanjima, Tokushima 770-8506, Japan

Abstract

This study was designed to determine the effectiveness of whole-body vibration (WBV) and intermittent parathyroid hormone (iPTH) in combination against estrogen deficiency-induced osteoporosis. Female C57BL/6J mice were bilaterally ovariectomized (OVX, n = 40) or sham-operated (sham-OVX, n = 8) at 9 weeks of age. Two weeks later, the OVX mice were randomly divided into four groups (n = 10 each): the control group (c-OVX) and groups treated with iPTH (p-OVX), WBV (w-OVX) and both (pw-OVX). The p-OVX and pw-OVX groups were given human PTH (1–34) at a dose of 30 µg/kg/day. The w-OVX and pw-OVX groups were exposed to WBV at an acceleration of 0.3 g and 45 Hz for 20 min/day. All mice were euthanized after the 18-day treatment, and the left tibiae were harvested. The proximal metaphyseal region was µCT-scanned, and its cortical bone cross-section was analyzed by Fourier transform infrared microspectroscopy and nanoindentation testing. A single application of iPTH or WBV to OVX mice had no effect on bone structure or material properties of cortical bone, which were compromised in comparison with those in sham-OVX mice. The combination of iPTH and WBV improved trabecular bone volume, thickness and connectivity in OVX mice. Although the combined treatment failed to improve cortical bone structure, its mineral maturity and hardness restored to the levels observed in sham-OVX mice. There was no evidence of interaction between the two treatments, and the combined effects seemed to be additive. These results suggest combining WBV with iPTH has potential for treating postmenopausal osteoporosis.

Keywords: postmenopausal osteoporosis, low-magnitude high-frequency vibration, parathyroid hormone, micro-computed tomography, infrared microspectroscopy, nanoindentation testing

Introduction

1 With the global aging population, osteoporosis has become an ever more important healthcare
2
3 issue in the elderly. Postmenopausal women, in particular, are frequently susceptible to osteoporosis
4
5 owing to a low peak bone mass coupled with menopausal bone loss. Worldwide there are more than 200
6
7 million women with postmenopausal osteoporosis [1, 2]. The X-ray diagnosis of the lumbar spine and the
8
9 femoral neck in a large-scale population-based cohort study in Japan [3, 4] revealed that 9.8 million
10
11 women aged 40 years and above suffered from osteoporosis. Osteoporosis increases bone fragility and
12
13 susceptibility to fracture and leads to increased morbidity and mortality as well as decreased functional
14
15 ability or quality of life. Therefore, the prevention and treatment of osteoporosis in postmenopausal
16
17 women have economic and health benefits.

18
19
20 In early postmenopausal women, estrogen deficiency increases bone turnover with a
21
22 prevalence of bone resorption over formation [5, 6]. A number of studies have focused on the efficacy of
23
24 anti-resorptive or anabolic pharmacological treatments for postmenopausal osteoporosis [7–9]. Of these
25
26 treatments, parathyroid hormone (PTH) is the first bone anabolic drug to be approved by the Food and
27
28 Drug Administration [10]. When injected once daily, PTH produces anabolic effects on the skeleton by
29
30 activating pro-differentiating and pro-survival signaling in osteoblastic cells [11]. This so-called
31
32 intermittent PTH (iPTH) induces an anabolic response in postmenopausal women [12, 13], and also in
33
34 ovariectomized (OVX) rodents [14, 15], which mimic postmenopausal bone loss [16].

35
36 Estrogen deficiency in postmenopausal osteoporosis alters estrogen receptor expressions [17,
37
38 18], thereby elevating bone mechano-responsiveness. Thus, mechanical stimuli may be potent
39
40 non-pharmacological alternatives for treating postmenopausal osteoporosis. In particular, whole body
41
42 vibration (WBV), which exposes subjects to low-intensity ($< 1 \times g$ in general; $g = 9.81 \text{ m/s}^2$),
43
44 high-frequency mechanical stimuli for short durations [19, 20], is more accessible than other loading
45
46 modalities for some elderly patients for whom exercising is contraindicated or difficult. Some evidence
47
48 has been reported for the mechano-responsiveness of sensitized bone to WBV [21] and for the
49
50 effectiveness of WBV against bone loss in OVX rodents [22, 23]. Postmenopausal women can also
51
52 benefit from WBV although its therapeutic outcome appears to be less pronounced in elderly than in
53
54 younger patients [24, 25].

55
56 Several studies have indicated that iPTH also sensitizes bone cells to mechanical stimuli and
57
58 lowers the bone-modeling threshold of mechanical strain, thereby enhancing mechanically stimulated
59
60

1 bone formation [26–28]. Furthermore, mechanical stimulation is thought to increase bone strength in an
2 efficient manner by localizing the anabolic effects of iPTH to biomechanically relevant sites [29, 30].
3
4 Considering these benefits of using iPTH and mechanical stimuli in combination, it is anticipated that the
5 concurrent use of WBV and iPTH will exert a synergistic or additive effect in preventing postmenopausal
6 bone loss. To our knowledge, however, there has been no study on the effect of WBV combined with
7 iPTH on postmenopausal osteoporosis. To address this shortcoming, we evaluated the effect of WBV,
8 iPTH, and their combination on OVX-induced osteoporosis in mice. Micro-computed tomography (μ CT),
9
10 Fourier transform infrared microspectroscopy (FTIR-MS), and nanoindentation testing were used to
11 assess bone structural, chemical, and mechanical properties, respectively.
12
13
14
15
16
17
18
19

20 **Method and Materials**

21 *General Procedures*

22 Experiments were conducted in accordance with the guiding principles of the American
23 Physiological Society and with the approval of the Animal Research Committee of Osaka University
24 Graduate School of Engineering Science.
25
26
27
28
29

30 Female C57BL/6J mice (CLEA Japan, Tokyo, Japan) were bilaterally ovariectomized (OVX, n
31 = 40) or sham-operated (sham-OVX, n = 8) under anesthesia by an intraperitoneal injection of ketamine
32 (100 mg/kg) and xylazine (10 mg/kg) at the age of 9 weeks. Mice were then single-housed in a plastic
33 cage under controlled conditions (12-hour light/dark cycle, 25°C, 60% humidity) and allowed free access
34 to a standard diet (CE-2; CLEA Japan) and tap water.
35
36
37
38
39

40 Two weeks later, the OVX mice were randomly divided into four groups (n = 10 each): the
41 control group (c-OVX) and the groups treated with WBV (w-OVX), iPTH (p-OVX) and WBV/iPTH
42 (pw-OVX). The p-OVX and pw-OVX groups were subcutaneously administered recombinant human
43 PTH (1–34) (Bachem California, Inc., Torrance, CA) dissolved in a vehicle of 0.2% bovine serum
44 albumin and 0.1% 1 mN hydrochloric acid in 0.9% saline to form a solution of 10 μ g/ml for delivery [31],
45 at a dose of 30 μ g/kg/day. The c-OVX, w-OVX and sham-OVX groups received the delivery vehicle only
46 at an equal volume to the p-OVX and pw-OVX groups. Additionally, mice in the w-OVX and pw-OVX
47 groups were put in a compartmented cage on the vibration platform (Big-Wave; Asahi Seisakujo, Tokyo,
48 Japan) and exposed daily to 20-min of vertical WBV at 45 Hz with a peak-to-peak acceleration of 0.3 g.
49 An earlier study reported the efficacy of WBV at this frequency and acceleration in the growing skeleton
50
51
52
53
54
55
56
57
58
59
60
61
62
63
64
65

1 of 8-week-old female mice [32]. Mice in the c-OVX, p-OVX, and sham-OVX groups were placed on the
2 vibration platform for 20 min but in a non-operating state. The vehicle or PTH was administered 30 min
3 before each WBV session. These interventions were introduced once daily at the same hour. After 18
4 days of treatment (one month after OVX), mice were euthanized by an overdose of pentobarbital sodium.
5 The left tibiae were harvested, dissected free of soft tissue, wrapped with moistened saline gauze, and
6 stored at -30°C until analysis.
7
8
9
10
11
12

13 *μCT Analysis*

14 The specimens were slowly thawed and then encapsulated in an acrylic tube filled with saline.
15
16 Next, the proximal part of the tibiae was scanned using a μCT system (SMX-1000/VCT; Shimadzu,
17 Kyoto, Japan). The scanning parameters were: 90 keV, 110 μA , 600-ms integration time and 1,200
18 projections over 360° . Image reconstruction was carried out for a 1.5-mm-long section of the metaphysis
19 distal to the growth plate (Fig. 1A), providing 167 contiguous slice images of cross-section composed of
20 512×512 , 9- μm cubic voxels with an 8-bit gray-scale resolution. Bone was segmented from background,
21 marrow or soft tissue residues by binarization using Otsu's method [33]. The outer and inner borders of
22 the cortical bone were determined by raster scanning in multiple directions after filling all bone pores, and
23 the trabecular and cortical compartments were segmented (Fig. 1B). The following structural indices were
24 determined: cortical bone volume (Cb.V, mm^3), medullary tissue volume (Mt.V, mm^3), cortical bone
25 thickness (Cb.Th, μm), trabecular bone volume fraction (Tb.Vf, %), trabecular bone thickness (Tb.Th,
26 μm), trabecular bone number (Tb.N, mm^{-1}) and trabecular bone connectivity density (Tb.Cd, mm^{-3}). A
27 three-dimensional method [34] was used for computing Cb.Th, Tb.Th and Tb.N. The BoneJ plugin 1.3.14
28 [35] for ImageJ 1.49v was used for calculating these indices.
29
30
31
32
33
34
35
36
37
38
39
40
41
42
43
44
45

46 *FTIR-MS*

47 After μCT , the proximal epimetaphyseal portion of the specimen was embedded in
48 polymethylmethacrylate (PMMA) without ethanol fixation to avoid possible deterioration of collagen
49 [36]. The longitudinal position showing the midsection of the metaphysis (Fig. 1A) was marked on the
50 cortical surface prior to embedding. After polymerization, using an 800-grit SiC abrasive paper disc, the
51 proximal surface of an embedded specimen was sanded perpendicularly to the tibial long axis in
52 deionized water until the position mark was reached. The surface was further polished sequentially with
53
54
55
56
57
58
59
60
61
62
63
64
65

1200- and 4000-grit abrasive paper discs, 1- μm diamond suspension (DP-Spray P; Struers, Ballerup, Denmark) and finally with 0.05- μm alumina suspension (AP-D; Struers, Ballerup, Denmark) to a state close to a mirror surface. The proximal cross section was ultrasonically cleaned to remove surface debris and heated at 50°C for 24 h in ambient air to prevent the enzymatic degradation of collagen [36].

The mirror-polished cortical cross-section was analyzed for chemicals using an FTIR-MS system (IRPrestige-21/AIM-8800; Shimadzu, Kyoto, Japan) in reflection mode. Spectra were collected from three $30 \times 30\text{-}\mu\text{m}^2$ regions, each at the anterior, posterior, medial and lateral cortices (Fig. 2A) under the conditions of 4 cm^{-1} spectral resolution and 50 scans per point. The data obtained were corrected for background and converted to absorbance units by the Kramers–Kronig transformation (Fig. 2B). The following chemical indices were determined: mineral/matrix ratio, estimated as the integrated area ratio of the phosphate band ($1,200\text{--}930\text{ cm}^{-1}$, baseline: $1,200\text{--}930\text{ cm}^{-1}$) to the amide I band ($1,720\text{--}1,600\text{ cm}^{-1}$, baseline: $1,720\text{--}1,600\text{ cm}^{-1}$); mineral maturity (the ratio of apatitic to non-apatitic phosphate), estimated as the area ratio $1,030\text{ cm}^{-1}$ over $1,020\text{ cm}^{-1}$ peaks (baseline: $1,200\text{--}930\text{ cm}^{-1}$); and collagen maturity (the ratio of non-reducible to reducible collagen cross-links), estimated as the area ratio $1,660\text{ cm}^{-1}$ over $1,690\text{ cm}^{-1}$ peaks (baseline: $1,720\text{--}1,600\text{ cm}^{-1}$). To resolve overlapping bands, the spectra were processed using PEAKFIT 4.12 (SeaSolve, San Jose, CA). Second derivative spectra, accompanied by 9-data-point Savitsky–Golay smoothing, were calculated to identify the peak wavenumbers of component bands in the spectra. These wavenumbers, which are in close agreement with published data [37, 38], were used for curve fitting with Gaussian component peaks. The position, half-bandwidth and amplitude of the peaks were altered until the resulting bands shifted by no more than 3 cm^{-1} from the initial parameters and good agreements between the sum of all components and the experimental spectra were achieved ($r^2 > 0.999$).

Nanoindentation testing

The PMMA-embedded specimens were subjected to nanoindentation testing by a dynamic ultra-micro-hardness tester (DUH-201S; Shimadzu, Kyoto, Japan) equipped with a diamond Berkovich tip; curvature radius $< 100\text{ nm}$. Three points were placed, maintaining a small distance from each other, in each square region where the chemical data were collected (Fig. 2A), and were tested with a trapezoidal loading waveform (Fig. 2C) having a maximum load of 6 mN with a loading/unloading rate of $300\text{ }\mu\text{N/s}$, giving a time-to-peak force of 20 s and a 100-s holding period at the maximum load [39]. Mechanical

indices were calculated from the resulting force (P)–displacement (h) curve according to the method of Oliver and Pharr [40].

The indentation modulus, as a function of the local elastic modulus E_{specimen} and Poisson ratio ν_{specimen} of the specimen, is given by

$$\text{indentation modulus} = \frac{E_{\text{specimen}}}{1 - \nu_{\text{specimen}}^2} = \left(\frac{1}{E_r} - \frac{1 - \nu_{\text{tip}}^2}{E_{\text{tip}}} \right)^{-1}, \quad (1)$$

where E_{tip} (1131 GPa) and ν_{tip} (0.07) are the elastic modulus and Poisson ratio of the diamond indenter, respectively, and E_r is the reduced modulus. The latter was derived from the slope of a tangent S at the point of initial unloading ($h = h_{\text{max}}$) and the contact area A_c , which have a direct relationship with E_r ,

$$S = S(h_{\text{max}}) = \left. \frac{dP}{dh} \right|_{h=h_{\text{max}}} = \frac{2}{\sqrt{\pi}} E_r \sqrt{A_c}. \quad (2)$$

The ratio of maximum force P_{max} (P at $h = h_{\text{max}}$) to A_c gives hardness, interpreted as a measure of strength, specifically resistance to non-elastic deformation under compression, i.e.,

$$\text{hardness} = \frac{P_{\text{max}}}{A_c} \quad (3)$$

Statistics

Data are presented as mean \pm standard deviation. Chemical and mechanical indices were averaged over measurement points in each specimen. One-way analysis of variance (ANOVA) with Tukey's post-hoc test was performed to analyze the difference between groups and two-way ANOVA to analyze the potential interaction between iPTH and WBV. Bartlett's test and the F -test showed no statistical differences in variances between groups in all data sets. All data were analyzed by Prism 6 (GraphPad Software; San Diego, CA), and a value of $P < 0.05$ was considered statistically significant.

Results

On the first day of interventions (2 weeks post-OVX), the c-OVX, p-OVX, w-OVX, pw-OVX and sham-OVX mice weighed 22.5 ± 0.8 , 22.8 ± 0.6 , 23.2 ± 0.9 , 23.1 ± 0.8 and 20.7 ± 1.0 g, respectively. Average body mass was 11% higher in OVX mice (c-OVX, p-OVX, w-OVX, pw-OVX) than in sham-OVX mice. On the last day of interventions (1 month post-OVX), the c-OVX, p-OVX, w-OVX and pw-OVX mice weighed 22.8 ± 1.1 , 22.8 ± 0.6 , 23.0 ± 0.8 and 23.3 ± 0.9 g, respectively, showing an average body mass 7% higher than the sham-OVX mice, which weighed 21.6 ± 0.5 g. Body mass did not

1 differ between c-OVX, p-OVX, w-OVX and pw-OVX, indicating no impact of iPTH, WBV and their
2 combination on body mass.

3
4 The representative three-dimensional reconstruction of tibial bone structure is illustrated for
5 each group in Fig. 1B, and the bone structural data are summarized in Table 1. All structural indices were
6 smaller in the c-OVX than in the sham-OVX mice. Compared with sham-OVX, p-OVX and w-OVX still
7 showed smaller values in all indices except for Tb.Cd in p-OVX, which, however, was similar to that in
8 c-OVX. No differences were found in Tb.Th and Tb.Cd between sham-OVX and pw-OVX, although
9 Tb.Vf, Tb.N and all cortical structural indices were still smaller in pw-OVX than in sham-OVX.
10 Furthermore, pw-OVX showed higher Tb.Vf and Tb.Cd than did c-OVX. There was no significant
11 interaction between WBV and iPTH for any structural index.
12
13
14
15
16
17
18
19

20 Table 2 presents chemical and mechanical properties of cortical bone. There were no
21 inter-group differences in mineral/matrix ratio or collagen maturity. Compared with sham-OVX, c-OVX
22 and p-OVX showed less mineral maturity. Mineral maturity was similar in w-OVX, pw-OVX, and
23 sham-OVX and was higher in pw-OVX than in c-OVX. Indentation modulus did not differ between
24 groups but showed a decreased tendency in c-OVX compared with sham-OVX ($P = 0.07$). Hardness was
25 smaller in c-OVX, p-OVX and w-OVX than in sham-OVX, higher in pw-OVX than in c-OVX, and
26 similar in sham-OVX and pw-OVX. No significant interaction was found between WBV and iPTH for
27 any chemical or mechanical index.
28
29
30
31
32
33
34
35

36 Figure 3 shows the plots of the mineral maturity and hardness for each specimen. Linear
37 regression analysis found a significant correlation in the pooled data of all groups but not within any
38 single group. No correlation was found in any of the other pairs of chemical and mechanical indices in
39 any group or the pooled data.
40
41
42
43
44
45

46 Discussion

47 This study was undertaken to determine whether the concurrent use of WBV and iPTH might
48 have therapeutic potential against osteoporosis in a synergistic or additive manner. A single application of
49 WBV or iPTH was not effective against osteoporotic bone loss in OVX mice. When the two treatments
50 were combined, however, OVX-induced reductions in trabecular bone volume and connectivity abated.
51 The efficacy of WBV and iPTH in combination was also observed in cortical bone hardness and mineral
52 maturity, both of which reduced in OVX mice but recovered to the healthy control levels. Considering
53
54
55
56
57
58
59
60
61
62
63
64
65

1 there was no interaction between the two treatments in any structure, chemical or mechanical index, the
2 combined treatment might be additive rather than synergistic.

3
4 Compared with sham-OVX mice, OVX mice showed smaller trabecular bone volume fraction,
5 thickness, number density and connectivity density. Cortical bone and medullary tissue volumes and
6 cortical thickness were also smaller in OVX mice than in sham-OVX mice. These declines in bone
7 structural indices in parallel with increased body mass are in line with previous studies using OVX mice
8 [14, 41–44], confirming the onset of osteoporosis one month after OVX treatment. In addition,
9 OVX-induced decreases in mineral maturity and hardness with a trend towards a declined indentation
10 modulus were observed at metaphyseal cortical bone. The increased proportion of immature crystals
11 observed here was also found in women during menopause [45], although there has been no study
12 documenting these chemical and mechanical properties in OVX mouse bone. The short-term effects of
13 OVX on intrinsic bone material properties have been examined only in femoral cortical bone of rabbits at
14 4 weeks post-OVX [46], which included a smaller mineral/matrix ratio, higher mineral maturity, higher
15 collagen maturity, lower indentation modulus and lower hardness compared with the age-matched healthy
16 rabbits. Differences to the present results, most notably the opposite trend for mineral maturity, could be
17 due to OVX models of different ages and species (young adult mice vs. mature adult rabbits) or skeletal
18 site-specific effects of OVX (tibial proximal metaphysis vs. femoral diaphysis) [47]. There are also
19 inconsistencies between other reports on the longer-term OVX effect on mineral maturity [46, 48, 49].

20
21 No significant difference was found in any structure, chemical or mechanical index between
22 untreated and iPTH-treated OVX mice, showing the insufficient anabolic effect of iPTH alone. In OVX
23 mice of the same strain, however, iPTH improved tibial bone mineral and structure [42, 50, 51]. In these
24 studies, the daily PTH (1–34) dose (40–80 µg/kg) was slightly higher, and durations to onset of iPTH
25 after OVX (4–6 weeks) and of iPTH treatment (3–4 weeks) were longer than those in the current study (2
26 weeks after OVX to onset of 30-µg/kg/day PTH over 18 days). On the other hand, a daily dose of
27 100-µg/kg PTH (1–84), equivalent to 40-µg/kg PTH (1–34), over 2 weeks after the introduction of OVX,
28 did not affect tibial bone structure in OVX mice of the same strain [52]. Differences in experimental time
29 frame or OVX-induced estrogen status [53] may be responsible for the variable anabolic efficacy of iPTH
30 in OVX mice.

31
32 Likewise, 18-day WBV alone was not effective against osteoporosis, although bone
33 mechano-responsiveness will be elevated in OVX-induced estrogen deficiency [21–23]. There have been

1 no studies investigating the effect of WBV in OVX mice. In a study exposing 8-week-old female BALB/c
2 mice to WBV (15 min/day, 5 day/week) with the same vibration settings as in the present work, Xie et al.
3 [32] showed a decline in osteoclastic activity in tibial trabecular bone and an increase in bone formation
4 rate on the tibial endocortical surface during the first 3 weeks. They also reported that another 3 weeks
5 were needed for the same daily WBV to yield significant effects in cortical bone geometry [54]. Chen et
6 al. treated 8-week-old OVX rats with a similar WBV protocol (45–55 Hz, 0.3 g; 20 min/day, 5 day/week),
7 starting the day after OVX introduction, and observed no effect during the first 4 weeks followed by
8 improvement of tibial trabecular bone structure during the next 8 weeks [55]. Thus, at least in the current
9 daily WBV protocol, a longer-term application would be required to produce skeletal changes in a
10 detectable fashion.
11
12
13
14
15
16
17
18
19

20 There has been only one study on the therapeutic potential of combining WBV with iPTH
21 against low-bone mass [56], in which 4- or 8-week concurrent use of WBV (90 Hz, 0.3 g; 15 min/day, 5
22 day/week) and iPTH (1–34) (10- or 40- μ g/kg/day) was shown to be no more effective than either single
23 use alone in tibiae of 7-month-old male BALB/c mice. In contrast, the present 18-day treatment of WBV
24 and iPTH in combination for OVX mice reduced osteoporotic trabecular bone loss and disconnectivity,
25 and restored cortical bone hardness and mineral maturity to the healthy control levels although either
26 treatment alone showed no skeletal effect. These outcomes may be due to the simultaneous elevation of
27 osteoblast number [11] and bone mechano-responsiveness [21-23] caused by iPTH and OVX-induced
28 low estrogen levels. The discrepancy between the two studies may also be attributed to differences in
29 WBV frequency, strains and age [57–59]. Cortical bone structure remained unaffected, even by the
30 combined treatment. A different metabolic turnover, which is faster for trabecular than for cortical bone
31 [60], may play a role in the different treatment outcomes in trabecular and cortical bone. A longer-term
32 study is needed to confirm the combined action of WBV and iPTH on cortical bone structure.
33
34
35
36
37
38
39
40
41
42
43
44
45

46 Early studies [61, 62] demonstrated the effectiveness of WBV in reducing high bone turnover
47 where bone resorption exceeds bone formation. Thus, iPTH-induced activation of WBV could lower bone
48 turnover or bone resorption that may be elevated because of OVX [5, 6]. A decrease in bone resorption
49 allows bone tissues to persist longer and favors bone maturation. Higher mineral maturity may be
50 associated with higher hardness in cortical bone of WBV/iPTH-treated OVX mice, as indicated by the
51 positive correlation between hardness and mineral maturity (Fig. 3). However, mineral maturity, defined
52 here as the ratio of apatitic to nonapatitic phosphate, evolves concomitantly with mineral crystal size and
53
54
55
56
57
58
59
60
61
62
63
64
65

1 crystalline perfection but possibly with different kinetics [63, 64]. Furthermore, other properties at the
2 crystal level, such as alignment of bone apatite crystallites and interactions between mineral and collagen,
3 will be involved in cortical bone hardness. Thus, although the combined treatment of WBV and iPTH
4 improved the material properties of bone tissue to the healthy control levels, further study is needed to
5 clarify the mechanisms by which chemical alterations to bone tissue affect their mechanical properties.
6
7

8
9
10 There are some limitations to be noted. First, we used only a single WBV protocol. The skeletal
11 effect of WBV varies with vibration frequency and magnitude [57, 65]. Thus, although no improvement
12 was found in bone structure or in material properties in WBV-treated OVX mice, there may be a more
13 favorable vibration setting for WBV to elicit therapeutic effects independently of iPTH or to provide
14 additional benefits when used concurrently with iPTH. Second, we used single-time-point data during
15 early-stage osteoporosis and assessed only short-term effects of treatments. Multi-time-point data over a
16 longer duration of osteoporosis are necessary for demonstrating the therapeutic efficacy of WBV and
17 iPTH in combination. Finally, we did not perform dynamic bone histomorphometry during treatments,
18 and therefore, we could not determine whether the WBV/iPTH-induced benefits to trabecular bone
19 structure were attributed to its anabolic or anti-catabolic action.
20
21

22
23
24 In conclusion, 18-day treatment of WBV combined with iPTH was additively effective in
25 improving trabecular bone structure and material properties of cortical bone at an early stage of
26 OVX-induced osteoporosis in mice, suggesting its potential for treating postmenopausal osteoporosis.
27 Further study is required for assessing its long-term therapeutic potential and for identifying an optimal
28 WBV protocol, possibly combined with a clinically feasible PTH dosage.
29
30
31
32
33
34
35
36
37
38
39
40
41
42
43
44
45
46
47
48
49
50
51
52
53
54
55
56
57
58
59
60
61
62
63
64
65

Acknowledgements

This work was supported in part by Grants in-Aid for Scientific Research from the Ministry of Education, Culture, Sports, Science and Technology of the Japanese government (grant numbers 24650265 and 26282120).

Ethical approval: All applicable international, national and/or institutional guidelines for the care and use of animals were followed. All procedures performed in studies involving animals were in accordance with the ethical standards of the institution or practice at which the studies were conducted.

Disclosure: None

References

1. (1993) Consensus development conference: diagnosis, prophylaxis, and treatment of osteoporosis. *Am J Med* 94:646–650
2. Lane NE (2006) Epidemiology, etiology, and diagnosis of osteoporosis. *Am J Obstet Gynecol* 194:S3-11
3. Yoshimura N, Muraki S, Oka H, Mabuchi A, En-Yo Y, Yoshida M, Saika A, Yoshida H, Suzuki T, Yamamoto S, Ishibashi H, Kawaguchi H, Nakamura K, Akune T (2009) Prevalence of knee osteoarthritis, lumbar spondylosis, and osteoporosis in Japanese men and women: the research on osteoarthritis/osteoporosis against disability study. *J Bone Miner Metab* 27:620–628
4. Yoshimura N, Muraki S, Oka H, Kawaguchi H, Nakamura K, Akune T (2010) Cohort profile: research on Osteoarthritis/Osteoporosis Against Disability study. *Int J Epidemiol* 39:988–995
5. Ravn P, Rix M, Andreassen H, Clemmesen B, Bidstrup M, Gunnes M (1997) High bone turnover is associated with low bone mass and spinal fracture in postmenopausal women. *Calcif Tissue Int* 60:255–260
6. D’Amelio P, Grimaldi A, Di Bella S, Brianza SZ, Cristofaro MA, Tamone C, Giribaldi G, Ulliers D, Pescarmona GP, Isaia G (2008) Estrogen deficiency increases osteoclastogenesis up-regulating T cells activity: a key mechanism in osteoporosis. *Bone* 43:92–100
7. Gaudio A, Morabito N (2005) Pharmacological management of severe postmenopausal osteoporosis. *Drugs Aging* 22:405–417
8. Papapoulos S, Makras P (2008) Selection of antiresorptive or anabolic treatments for postmenopausal osteoporosis. *Nat Clin Pract Endocrinol Metab* 4:514–523
9. Gallacher SJ, Dixon T (2010) Impact of treatments for postmenopausal osteoporosis (bisphosphonates, parathyroid hormone, strontium ranelate, and denosumab) on bone quality: a systematic review. *Calcif Tissue Int* 87:469–484
10. Qin L, Raggatt LJ, Partridge NC (2004) Parathyroid hormone: a double-edged sword for bone metabolism. *Trends Endocrinol Metab* 15:60–65
11. Jilka RL (2007) Molecular and cellular mechanisms of the anabolic effect of intermittent PTH. *Bone* 40:1434–1446
12. Fox J, Miller MA, Recker RR, Bare SP, Smith SY, Moreau I (2005) Treatment of postmenopausal osteoporotic women with parathyroid hormone 1-84 for 18 months increases cancellous bone

- formation and improves cancellous architecture: a study of iliac crest biopsies using histomorphometry and micro computed tomography. *J Musculoskelet Neuronal Interact* 5:356–357
13. Senn C, Günther B, Popp AW, Perrelet R, Hans D, Lippuner K (2014) Comparative effects of teriparatide and ibandronate on spine bone mineral density (BMD) and microarchitecture (TBS) in postmenopausal women with osteoporosis: a 2-year open-label study. *Osteoporos Int* 25:1945–1951
14. Alexander JM, Bab I, Fish S, Müller R, Uchiyama T, Gronowicz G, Nahounou M, Zhao Q, White DW, Chorev M, Gazit D, Rosenblatt M (2001) Human parathyroid hormone 1-34 reverses bone loss in ovariectomized mice. *J Bone Miner Res* 16:1665–1673
15. Fox J, Miller MA, Newman MK, Metcalfe AF, Turner CH, Recker RR, Smith SY (2006) Daily treatment of aged ovariectomized rats with human parathyroid hormone (1-84) for 12 months reverses bone loss and enhances trabecular and cortical bone strength. *Calcif Tissue Int* 79:262–272
16. Kalu DN (1991) The ovariectomized rat model of postmenopausal bone loss. *Bone Miner* 15:175–191
17. Aguirre JI, Plotkin LI, Gortazar AR, Millan MM, O'Brien CA, Manolagas SC, Bellido T (2007) A novel ligand-independent function of the estrogen receptor is essential for osteocyte and osteoblast mechanotransduction. *J Biol Chem* 282:25501–25508
18. Wehrle E, Liedert A, Heilmann A, Wehner T, Bindl R, Fischer L, Haffner-Luntzer M, Jakob F, Schinke T, Amling M, Ignatius A (2015) The impact of low-magnitude high-frequency vibration on fracture healing is profoundly influenced by the oestrogen status in mice. *Dis Model Mech* 8:93–104
19. Prisby RD, Lafage-Proust MH, Malaval L, Belli A, Vico L (2008) Effects of whole body vibration on the skeleton and other organ systems in man and animal models: what we know and what we need to know. *Ageing Res Rev* 7:319–329
20. Slatkovska L, Alibhai SM, Beyene J, Cheung AM (2010) Effect of whole-body vibration on BMD: a systematic review and meta-analysis. *Osteoporos Int* 21:1969–1980
21. Rubinacci A, Marenzana M, Cavani F, Colasante F, Villa I, Willnecker J, Moro GL, Spreafico LP, Ferretti M, Guidobono F, Marotti G (2008) Ovariectomy sensitizes rat cortical bone to whole-body vibration. *Calcif Tissue Int* 82:316–326
22. Oxlund BS, Ørtoft G, Andreassen TT, Oxlund H (2003) Low-intensity, high-frequency vibration appears to prevent the decrease in strength of the femur and tibia associated with ovariectomy of adult rats. *Bone* 32:69–77

- 1
2
3
4
5
6
7
8
9
10
11
12
13
14
15
16
17
18
19
20
21
22
23
24
25
26
27
28
29
30
31
32
33
34
35
36
37
38
39
40
41
42
43
44
45
46
47
48
49
50
51
52
53
54
55
56
57
58
59
60
61
62
63
64
65
23. Zhou Y, Guan X, Liu T, Wang X, Yu M, Yang G, Wang H (2015) Whole body vibration improves osseointegration by up-regulating osteoblastic activity but down-regulating osteoblast-mediated osteoclastogenesis via ERK1/2 pathway. *Bone* 71:17–24
 24. Rubin C, Recker R, Cullen D, Ryaby J, McCabe J, McLeod K (2004) Prevention of postmenopausal bone loss by a low-magnitude, high-frequency mechanical stimuli: a clinical trial assessing compliance, efficacy, and safety. *J Bone Miner Res* 19:343–351
 25. Kiel DP, Hannan MT, Barton BA, Bouxsein ML, Sisson E, Lang T, Allaire B, Dewkett D, Carroll D, Magaziner J, Shane E, Leary ET, Zimmerman S, Rubin CT (2015) Low-magnitude mechanical stimulation to improve bone density in persons of advanced age: a randomized, placebo-controlled trial. *J Bone Miner Res* 30:1319–1328
 26. Chow JW, Fox S, Jagger CJ, Chambers TJ (1998) Role for parathyroid hormone in mechanical responsiveness of rat bone. *Am J Physiol* 274:E146–154
 27. Hagino H, Okano T, Akhter MP, Enokida M, Teshima R (2001) Effect of parathyroid hormone on cortical bone response to in vivo external loading of the rat tibia. *J Bone Miner Metab* 19:244–250
 28. Kim CH, Takai E, Zhou H, von Stechow D, Müller R, Dempster DW, Guo XE (2003) Trabecular bone response to mechanical and parathyroid hormone stimulation: the role of mechanical microenvironment. *J Bone Miner Res* 18:2116–2125
 29. Roberts MD, Santner TJ, Hart RT (2009) Local bone formation due to combined mechanical loading and intermittent hPTH-(1-34) treatment and its correlation to mechanical signal distributions. *J Biomech* 42:2431–2438
 30. McAteer ME, Niziolek PJ, Ellis SN, Alge DL, Robling AG (2010) Mechanical stimulation and intermittent parathyroid hormone treatment induce disproportional osteogenic, geometric, and biomechanical effects in growing mouse bone. *Calcif Tissue Int* 86:389–396
 31. Warden SJ, Komatsu DE, Rydberg J, Bond JL, Hassett SM (2009) Recombinant human parathyroid hormone (PTH 1-34) and low-intensity pulsed ultrasound have contrasting additive effects during fracture healing. *Bone* 44:485–494
 32. Xie L, Jacobson JM, Choi ES, Busa B, Donahue LR, Miller LM, Rubin CT, Judex S (2006) Low-level mechanical vibrations can influence bone resorption and bone formation in the growing skeleton. *Bone* 39:1059–1066

- 1
2
3
4
5
6
7
8
9
10
11
12
13
14
15
16
17
18
19
20
21
22
23
24
25
26
27
28
29
30
31
32
33
34
35
36
37
38
39
40
41
42
43
44
45
46
47
48
49
50
51
52
53
54
55
56
57
58
59
60
61
62
63
64
65
33. Otsu N (1979) Threshold selection method from gray-level histograms. *IEEE Trans Syst Man Cybern* 9:62–66
 34. Hildebrand T, Ruegsegger P (1997) A new method for the model-independent assessment of thickness in three-dimensional images. *Journal of Microscopy-Oxford* 185:67–75
 35. Doube M, Klosowski MM, Arganda-Carreras I, Cordelières FP, Dougherty RP, Jackson JS, Schmid B, Hutchinson JR, Shefelbine SJ (2010) BoneJ: Free and extensible bone image analysis in ImageJ. *Bone* 47:1076–1079
 36. Hengsberger S, Kulik A, Zysset P (2002) Nanoindentation discriminates the elastic properties of individual human bone lamellae under dry and physiological conditions. *Bone* 30:178–184
 37. Dong A, Huang P, Caughey WS (1990) Protein secondary structures in water from second-derivative amide I infrared spectra. *Biochemistry* 29:3303–3308
 38. Gadaleta SJ, Paschalis EP, Betts F, Mendelsohn R, Boskey AL (1996) Fourier transform infrared spectroscopy of the solution-mediated conversion of amorphous calcium phosphate to hydroxyapatite: new correlations between X-ray diffraction and infrared data. *Calcif Tissue Int* 58:9–16
 39. Silva MJ, Brodt MD, Fan Z, Rho JY (2004) Nanoindentation and whole-bone bending estimates of material properties in bones from the senescence accelerated mouse SAMP6. *J Biomech* 37:1639–1646
 40. Oliver W, Pharr G (2004) Measurement of hardness and elastic modulus by instrumented indentation: Advances in understanding and refinements to methodology. *Journal of Materials Research* 19:3–20
 41. Andersson N, Lindberg MK, Ohlsson C, Andersson K, Ryberg B (2001) Repeated in vivo determinations of bone mineral density during parathyroid hormone treatment in ovariectomized mice. *J Endocrinol* 170:529–537
 42. Zhou H, Iida-Klein A, Lu SS, Ducayen-Knowles M, Levine LR, Dempster DW, Lindsay R (2003) Anabolic action of parathyroid hormone on cortical and cancellous bone differs between axial and appendicular skeletal sites in mice. *Bone* 32:513–520
 43. Xiang A, Kanematsu M, Mitamura M, Kikkawa H, Asano S, Kinoshita M (2006) Analysis of change patterns of microcomputed tomography 3-dimensional bone parameters as a high-throughput

- 1
2
3
4
5
6
7
8
9
10
11
12
13
14
15
16
17
18
19
20
21
22
23
24
25
26
27
28
29
30
31
32
33
34
35
36
37
38
39
40
41
42
43
44
45
46
47
48
49
50
51
52
53
54
55
56
57
58
59
60
61
62
63
64
65
- tool to evaluate antiosteoporotic effects of agents at an early stage of ovariectomy-induced osteoporosis in mice. *Invest Radiol* 41:704–712
44. Rogers NH, Perfield JW, Strissel KJ, Obin MS, Greenberg AS (2009) Reduced energy expenditure and increased inflammation are early events in the development of ovariectomy-induced obesity. *Endocrinology* 150:2161–2168
45. Farlay D, Bala Y, Bare S, Lappe J, Recker R, Boivin G (2012) Modifications of bone material properties early detected after one year of menopause in women. *J Bone Miner Res* 27:FR 0144
46. Wen XX, Wang FQ, Xu C, Wu ZX, Zhang Y, Feng YF, Yan YB, Lei W (2015) Time related changes of mineral and collagen and their roles in cortical bone mechanics of ovariectomized rabbits. *PLoS One* 10:e0127973
47. Zhang Y, Lai WP, Leung PC, Wu CF, Wong MS (2007) Short- to mid-term effects of ovariectomy on bone turnover, bone mass and bone strength in rats. *Biol Pharm Bull* 30:898–903
48. Brennan O, Kuliwaba JS, Lee TC, Parkinson IH, Fazzalari NL, McNamara LM, O'Brien FJ (2012) Temporal changes in bone composition, architecture, and strength following estrogen deficiency in osteoporosis. *Calcif Tissue Int* 91:440–449
49. Mathavan N, Turunen MJ, Tägil M, Isaksson H (2015) Characterising bone material composition and structure in the ovariectomized (OVX) rat model of osteoporosis. *Calcif Tissue Int* 97:134–144
50. Pierroz DD, Bouxsein ML, Rizzoli R, Ferrari SL (2006) Combined treatment with a beta-blocker and intermittent PTH improves bone mass and microarchitecture in ovariectomized mice. *Bone* 39:260–267
51. Yamane H, Sakai A, Mori T, Tanaka S, Moridera K, Nakamura T (2009) The anabolic action of intermittent PTH in combination with cathepsin K inhibitor or alendronate differs depending on the remodeling status in bone in ovariectomized mice. *Bone* 44:1055–1062
52. Roche B, Vanden-Bossche A, Malaval L, Normand M, Jannot M, Chau R, Vico L, Lafage-Proust MH (2014) Parathyroid hormone 1-84 targets bone vascular structure and perfusion in mice: impacts of its administration regimen and of ovariectomy. *J Bone Miner Res* 29:1608–1618
53. Masiukiewicz US, Mitnick M, Grey AB, Insogna KL (2000) Estrogen modulates parathyroid hormone-induced interleukin-6 production in vivo and in vitro. *Endocrinology* 141:2526–2531
54. Xie L, Rubin C, Judex S (2008) Enhancement of the adolescent murine musculoskeletal system using low-level mechanical vibrations. *J Appl Physiol* (1985) 104:1056–1062

- 1
2
3
4
5
6
7
8
9
10
11
12
13
14
15
16
17
18
19
20
21
22
23
24
25
26
27
28
29
30
31
32
33
34
35
36
37
38
39
40
41
42
43
44
45
46
47
48
49
50
51
52
53
54
55
56
57
58
59
60
61
62
63
64
65
55. Chen GX, Zheng S, Qin S, Zhong ZM, Wu XH, Huang ZP, Li W, Ding RT, Yu H, Chen JT (2014) Effect of low-magnitude whole-body vibration combined with alendronate in ovariectomized rats: a random controlled osteoporosis prevention study. *PLoS One* 9:e96181
 56. Lynch MA, Brodt MD, Stephens AL, Civitelli R, Silva MJ (2011) Low-magnitude whole-body vibration does not enhance the anabolic skeletal effects of intermittent PTH in adult mice. *J Orthop Res* 29:465–472
 57. Judex S, Lei X, Han D, Rubin C (2007) Low-magnitude mechanical signals that stimulate bone formation in the ovariectomized rat are dependent on the applied frequency but not on the strain magnitude. *J Biomech* 40:1333–1339
 58. Lynch MA, Brodt MD, Silva MJ (2010) Skeletal effects of whole-body vibration in adult and aged mice. *J Orthop Res* 28:241–247
 59. Klinck J, Boyd SK (2008) The magnitude and rate of bone loss in ovariectomized mice differs among inbred strains as determined by longitudinal in vivo micro-computed tomography. *Calcif Tissue Int* 83:70–79
 60. Parfitt AM (1983) The physiologic and clinical significance of bone histomorphometric data. In: Recker R (ed) *Bone Histomorphometry. Techniques and Interpretations*. CRC Press, Boca Raton, pp 143–223
 61. Turner S, Torode M, Climstein M, Naughton G, Greene D, Baker MK, Fiatarone Singh MA (2011) A randomized controlled trial of whole body vibration exposure on markers of bone turnover in postmenopausal women. *J Osteoporos* 2011:710387
 62. Wei QS, Wang HB, Wang JL, Fang B, Zhou GQ, Tan X, He W, Deng WM (2015) Combination treatment with whole body vibration and a kidney-tonifying herbal Fufang prevent osteoporosis in ovariectomized rats. *Orthop Surg* 7:57–65
 63. Farlay D, Panczer G, Rey C, Delmas PD, Boivin G (2010) Mineral maturity and crystallinity index are distinct characteristics of bone mineral. *J Bone Miner Metab* 28:433–445
 64. Bala Y, Farlay D, Boivin G (2013) Bone mineralization: from tissue to crystal in normal and pathological contexts. *Osteoporos Int* 24:2153–2166
 65. Christiansen BA, Silva MJ (2006) The effect of varying magnitudes of whole-body vibration on several skeletal sites in mice. *Ann Biomed Eng* 34:1149–1156

Table 1 Bone structural indices

	sham-OVX	c-OVX	p-OVX	w-OVX	pw-OVX
Tb.Vf [%]	8.96±1.58	6.00±0.64 ^a	6.84±0.78 ^a	6.68±0.51 ^a	7.21±0.46 ^{a,b}
Tb.Th [µm]	44.2±4.0	40.4±2.1 ^a	41.0±2.2 ^a	40.9±1.9 ^a	41.7±1.1
Tb.N [mm ⁻³]	1496±229	1054±143 ^a	1145±184 ^a	1101±161 ^a	1225±200 ^a
Tb.Cd [mm ⁻³]	173.2±44.1	92.7±38.0 ^a	128.1±42.7	118.2±33.8 ^a	144.3±37.3 ^b
Cb.V [mm ³]	1.38±0.16	1.08±0.09 ^a	1.11±0.07 ^a	1.10±0.07 ^a	1.17±0.05 ^a
Cb.Th [µm]	128.5±10.4	106.9±7.5 ^a	110.6±8.5 ^a	107.1±7.2 ^a	111.6±5.6 ^a
Mt.V [mm ³]	3.22±0.46	2.52±0.13 ^a	2.46±0.13 ^a	2.50±0.12 ^a	2.55±0.13 ^a

^a*P*<0.05 vs. sham-OVX, ^b*P*<0.05 vs. c-OVX

1
2
3
4
5
6
7
8
9
10
11
12
13
14
15
16
17
18
19
20
21
22
23
24
25
26
27
28
29
30
31
32
33
34
35
36
37
38
39
40
41
42
43
44
45
46
47
48
49
50
51
52
53
54
55
56
57
58
59
60
61
62
63
64
65

Table 2 Chemical and mechanical properties of cortical bone

	sham-OVX	c-OVX	p-OVX	w-OVX	pw-OVX
mineral/matrix ratio	7.80±0.74	7.67±0.99	8.32±0.96	8.08±0.85	7.92±0.68
mineral maturity	1.57±0.14	1.27±0.15 ^a	1.30±0.19 ^a	1.39±0.13	1.51±0.21 ^b
collagen maturity	5.71±1.11	4.64±1.01	5.07±1.42	4.75±1.15	4.97±1.43
indentation modulus [GPa]	17.95±2.90	13.72±4.81	15.71±2.39	14.94±2.15	15.39±3.57
hardness [GPa]	1.05±0.25	0.57±0.19 ^a	0.75±0.11 ^a	0.74±0.08 ^a	0.90±0.16 ^b

^a*P*<0.05 vs. sham-OVX, ^b*P*<0.05 vs. c-OVX

Figure captions

1
2
3
4
5
6
7
8
9
10
11
12
13
14
15
16
17
18
19
20
21
22
23
24
25
26
27
28
29
30
31
32
33
34
35
36
37
38
39
40
41
42
43
44
45
46
47
48
49
50
51
52
53
54
55
56
57
58
59
60
61
62
63
64
65

Figure 1. (A) Projection of the reconstructed three-dimensional volume of proximal tibial bone, showing a region for structural analysis defined by a volume extending a distance of 1.5 mm distal to the growth plate. Dashed line shows the transverse section evaluated for FTIR-MS and nanoindentation testing. (B) Three-dimensional metaphyseal tibial images, segmented into trabecular and cortical bone. Images were selected from mice having near-mean values of trabecular bone volume fraction in each group

Figure 2. (A) Metaphyseal cross-sectional image at a polished cut surface, showing regions for FTIR-MS and indents by nanoindentation testing. Each of four regions measured for FTIR spectra include three indents. (B, C) Examples of FTIR spectra after 9-data-point smoothing and baseline correction (left) and a force–displacement curve during a loading-holding-unloading process (right)

Figure 3. Plots of hardness vs. mineral maturity. Each plot represents the mean of all data in a single specimen. Pooled data show the significant correlation between hardness and mineral maturity

1
2
3
4
5
6
7
8
9
10
11
12
13
14
15
16
17
18
19
20
21
22
23
24
25
26
27
28
29
30
31
32
33
34
35
36
37
38
39
40
41
42
43
44
45
46
47
48
49
50
51
52
53
54
55
56
57
58
59
60
61
62
63
64
65

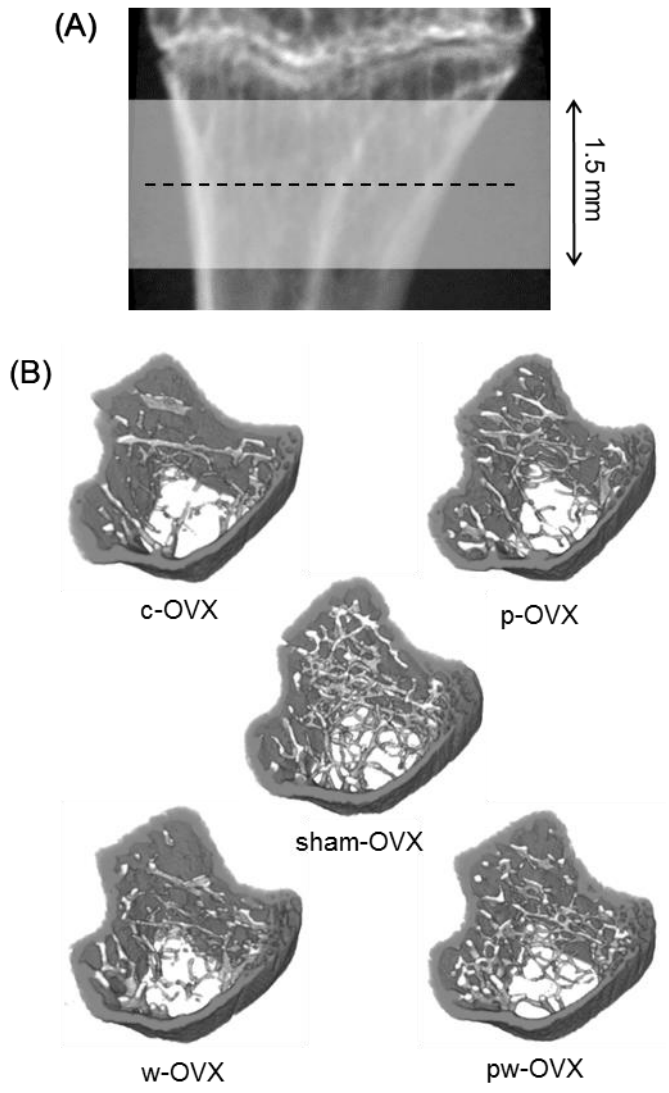


Fig. 1

1
2
3
4
5
6
7
8
9
10
11
12
13
14
15
16
17
18
19
20
21
22
23
24
25
26
27
28
29
30
31
32
33
34
35
36
37
38
39
40
41
42
43
44
45
46
47
48
49
50
51
52
53
54
55
56
57
58
59
60
61
62
63
64
65

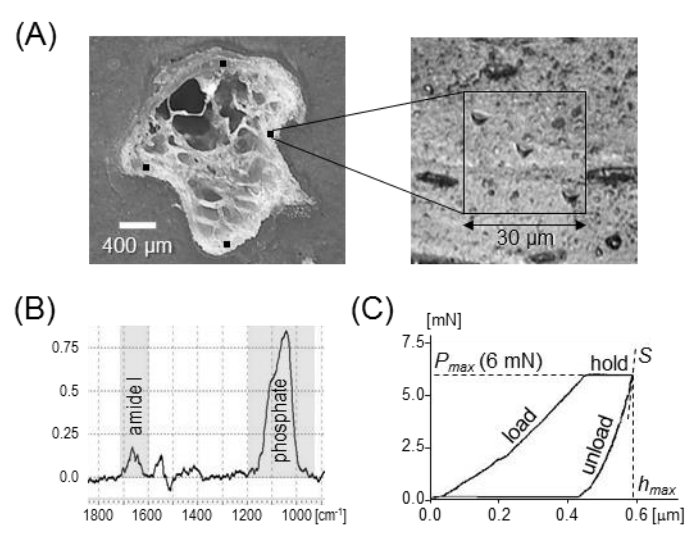


Fig. 2

1
2
3
4
5
6
7
8
9
10
11
12
13
14
15
16
17
18
19
20
21
22
23
24
25
26
27
28
29
30
31
32
33
34
35
36
37
38
39
40
41
42
43
44
45
46
47
48
49
50
51
52
53
54
55
56
57
58
59
60
61
62
63
64
65

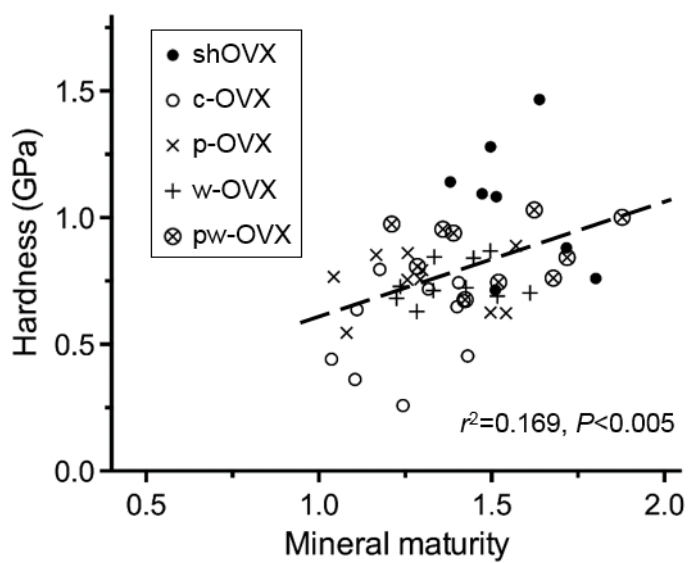


Fig. 3